J Sol-Gel Sci Technol (2017) 84:522–534
DOI 10.1007/s10971-017-4426-8

INVITED PAPER: SOL-GEL AND HYBRID MATERIALS FOR OPTICAL, PHOTONIC AND OPTOELECTRONIC APPLICATIONS

Total internal reflection-based optofluidic waveguides fabricated in aerogels

Yaprak Özbakır[1,2] · Alexandr Jonáš[3] · Alper Kiraz[2,4] · Can Erkey[1]

Received: 9 December 2016 / Accepted: 16 May 2017 / Published online: 6 June 2017

Abstract Liquid-core optofluidic waveguides based on total internal reflection of light were built in water-filled cylindrical microchannels fabricated in hydrophobic silica aerogels. Silica aerogels with densities ranging from 0.15 to 0.39 g/cm^3 were produced by aging of alcogels in tetraethylorthosilicate solution for various time periods, followed by supercritical extraction of the solvent from the alcogel network. Subsequently, the resulting hydrophilic aerogel samples were made hydrophobic by hexamethyldisilazane vapor treatment. The synthesized samples retained their low refractive index (below ~1.09) and, hence, they could serve as suitable optical cladding materials for aqueous waveguide cores (refractive index $n_{core} = 1.33$). Hydrophobic silica aerogel samples produced by the above technique also had low absorption coefficients in the visible part of the spectrum. Fabrication of microchannels in aerogel blocks by manual drilling preserving nanoporous and monolithic structure of aerogels was demonstrated for the first time. Long channels (up to ~7.5 cm) with varying geometries such as straight and inclined *L*-shaped channels could be fabricated. Multimode optofluidic waveguides prepared by filling the channels in the drilled aerogel monoliths with water yielded high numerical aperture values (~0.8). Efficient guiding of light by total internal reflection in the water-filled channels in aerogels was visually revealed and characterized by monitoring the channel output. The presented technique is expected to open up further possibilities for creating three-dimensional networks of liquid channels in aerogels for optofluidic applications.

Graphical Abstract

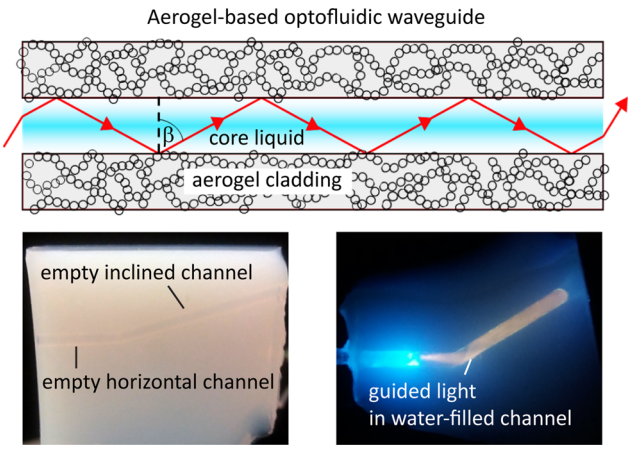

1 Introduction

Optofluidic devices are obtained by integrating microfluidic technology with optical structures in such a way that light and fluids occupy a common space [1, 2]. Optofluidic

✉ Can Erkey
cerkey@ku.edu.tr

1 Department of Chemical and Biological Engineering, Koc University, 34450 Sarıyer, Istanbul, Turkey

2 Department of Physics, Koc University, 34450 Sarıyer, Istanbul, Turkey

3 Department of Physics, Istanbul Technical University, 34469 Maslak, Istanbul, Turkey

4 Department of Electrical and Electronics Engineering, Koc University, 34450 Sarıyer, Istanbul, Turkey

waveguides used for efficient capture and controlled delivery of electromagnetic radiation from a source to a target represent one of the basic building blocks of such devices. The waveguides can be used in light-driven processes including photometric and spectroscopic analysis of minute sample volumes and energy production based on conversion of light energy in photochemical reactions [2–5]. Among various optofluidic waveguides, total internal reflection (TIR)-based liquid-core waveguides enable the most straightforward way for guiding and controlled routing of light and have become an important platform that has received an increasing recognition and utilization in a wide range of applications, such as chemical and biological sensing and analysis [6–13], energy conversion [14] as well as imaging [15]. Such liquid-core waveguides are composed of a liquid filled channel in a suitable solid material which acts as waveguide cladding [16, 17]. For the propagation of non-lossy optical modes guided in the core liquid by total internal reflection, cladding material should have a low absorption coefficient and should also have a lower refractive index than that of the core liquid ($n_{core} > n_{cladding}$) [17–21].

In applications involving aqueous solutions, the refractive index of the core liquid is around 1.33 (refractive index of water). However, a limited choice of solid host materials with an index of refraction below that of water is available; thus it is a challenge to find a cladding material with a refractive index sufficiently lower than 1.33 to maintain a reasonable numerical aperture (NA) [22, 23]. Most of the polymers, including those that are utilized in lab-on-a-chip devices such as polydimethylsiloxane (PDMS), have higher refractive indices than water; thus, light cannot be confined and delivered by TIR in channels fabricated from these polymers. Among fluoropolymers, amorphous fluoropolymer (Teflon AF) has a refractive index of 1.29–1.31 that is slightly lower than the refractive index of water. Therefore, Teflon AF or a layer of Teflon AF can be used to clad a liquid-core optical waveguide. For example, Datta et al. fabricated a TIR-based liquid-core optical waveguide device for absorbance measurements and fluorescence detection [24]. The microchannels for confining the core liquid were constructed by wet etching of a silicon wafer. Because the refractive index of the silicon substrate ($n = 3.98$) is higher than that of the aqueous solution, the channel surfaces were coated by Teflon AF to enable TIR. The absorbance of dye compounds in solutions with concentrations varying in the range of 2 to 100 µM could be successfully measured and related quantitatively to the concentration of the sample. In addition, fluorescent dyes contained within the microchannel could be detected down to nanomolar concentrations. Similarly, Wu and Gong designed a monolithic PDMS-based sensor for the detection of nitrite concentration in aqueous solutions using TIR [25]. The microchannels were fabricated from PDMS ($n = 1.4$) and the channel surfaces were coated by Teflon AF. After filling the open-ended channel by an aqueous nitrite solution, light was coupled into the channel by the aid of an optical fiber. Subsequently, light could be guided through the liquid-filled channel and detected at the end of the channel by an absorption spectrophotometer. The concentration of the sample could be measured from the absorbance. Jung et al. integrated a TIR-based liquid-core optofluidic waveguide into a PDMS-based photobioreactor (PBR) for light delivery to cyanobacteria [14]. The waveguides were constructed by coating a thin layer of Teflon AF on the inner walls of PDMS fluidic channels containing the culture medium ($n_{core} = 1.332$). They demonstrated enhancement of cell growth by the aid of optofluidic waveguide-based PBR compared to a regular PBR without waveguiding structures.

Even though the above-mentioned studies indicate the potential of TIR-based optofluidics waveguides, Teflon AF is not an optimal material for optofluidic applications as it has poor adhesion to the common solid substrates used for manufacturing of microfluidic chips. Chemical functionalization of the surface of Teflon AF may improve adhesion, but it is very difficult to functionalize Teflon AF. Furthermore, low refractive index contrast of ~0.04 between the core liquid and Teflon AF prevents efficient propagation of light within the aqueous core [26, 27]. Therefore, materials with a refractive index much lower than 1.33 are needed for further development of TIR-based waveguides.

Aerogels are nanostructured materials with an internal solid structure consisting of crosslinked polymers with a large number of air-filled pores between the solid polymeric chains [28, 29]. They can be produced as macroscopic monoliths with unique properties such as high surface area, narrow pore size distribution and high pore volume. Due to their very high porosities, they are sometimes called “solid air” and have refractive indices close to that of air which makes them remarkable solid-cladding materials [20, 28, 30]. As depicted in Fig. 1, light coupled into a liquid-filled microchannel in an aerogel surrounded by a wall made up of interconnected nanoparticles with air pockets in the pores between them can be confined and guided through the channel by total internal reflection [23, 31, 32].

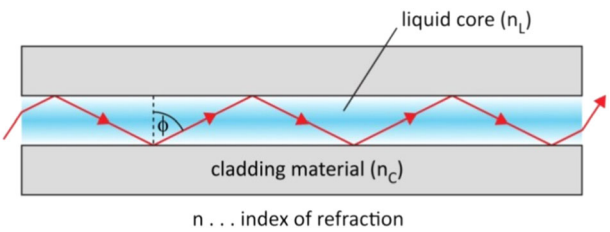

Fig. 1 Liquid-core optofluidic waveguides in microchannels

Aerogel-based optofluidic waveguides are fabricated by opening microchannels in aerogel monoliths. There exist several possible strategies for fabricating uniform, extended channels in hydrophobic aerogel blocks. Xiao et al. demonstrated for the first time that water-filled microchannels in silica aerogel blocks can be used as optical waveguides [31]. To create a microchannel in an aerogel block, a solution of tetraethylorthosilicate (TEOS), water, and ethanol was poured into a mold in which an optical fiber was placed. After gelation of the solution and supercritical drying of the gel, the fiber was carefully pulled out of the aerogel block leaving a fiber-sized microchannel within the block. The microchannel was then filled with water. Upon coupling the light into the water-filled channel, light guiding could be demonstrated. However, withdrawal of the fiber embedded in the aerogel frequently leads to breakage due to adhesion of the fiber to the silica aerogel network. Furthermore, only straight channels can be formed using this technique and it is not possible to form channels with complex geometries.

Eris et al. developed a new method to fabricate channels in aerogels based on embedding a fiber made of trifluoropropyl polyhedral oligomeric silsesquioxane (trifluoropropyl POSS) in the wet aerogel precursor [32]. First, a *U*-shaped trifluoropropyl POSS fiber prepared by melt/freeze processing was placed into a solution of TEOS, water and ethanol. After gelation and aging of the alcogel with embedded POSS fiber, $scCO_2$ extraction was used to dry the alcogel and extract the POSS fiber, yielding a silica aerogel with a *U*-shaped empty channel inside. Using this technique, breaking of the aerogel can be prevented and it may also be possible to form channels with complex geometries in the aerogel blocks. However, trifluoropropyl POSS is not easily moldable into complex geometries and there does not seem to be any moldable polymers which are soluble in $scCO_2$ and insoluble in the solvents and solvent mixtures used in sol–gel processing.

Another alternative for fabricating channels in monolithic aerogel blocks is laser processing. Bian et al. sliced cylindrical polyurea aerogel samples of 10–15 mm in diameter into 1–3 mm disks by laser ablation using femtosecond laser pulses [33]. The laser beam at 800 nm was focused at the center of the sample which was placed on a micro-positioning stage so that the sample could be rotated or translated in 3D for cutting. Inspired by this demonstration of laser processing of monolithic aerogels, Yalızay et al. used femtosecond laser ablation to create TIR-based liquid-core optofluidic waveguides in hydrophobic silica aerogel monoliths [23]. In their experiments, the laser beam was focused on the sample surface and essentially vaporized the silica. Desired cross-section of the channel was achieved by scanning the ablation beam focus across the aerogel surface in the *x* and *y* directions. Simultaneously with the *x*–*y* scanning, the sample was translated along the *z*-axis by a micro-positioning stage. This resulted in cylindrical microchannels fabricated inside the silica aerogel blocks. However, this method only enables manufacturing of straight optofluidic waveguides with uniform cross-section that are very short (only a few millimeter length).

In this study, we present a new, straightforward technique that uses direct manual drilling to manufacture TIR-based liquid-core optofluidic waveguides in aerogel monoliths. This method is capable of producing channels with lengths significantly larger than those reported previously in the literature and it also provides relative flexibility in the channel shaping. To illustrate the potential of our technique, we demonstrate that both a straight channel and an *L*-shaped channel with the total length up to ~7.5 cm could be created. The resulting aerogel-based optofluidic waveguides exhibited efficient light guiding features, as verified by direct imaging of guided light modes and measuring the transmittance of the waveguides.

2 Materials and methods

2.1 Preparation of silica aerogel monoliths

Silica aerogels were synthesized using a conventional two step sol–gel process and aged in TEOS-containing aging solutions as shown in Fig. 2. TEOS (98% purity; AlfaAesar) was used as the silica precursor, hydrochloric acid (HCl) (37% purity; Riedel-de Haen) as the acid catalyst, and ammonium hydroxide (NH_4OH) (2.0 M in ethanol; Aldrich) as the base catalyst. TEOS, ethanol (99.9% purity; Merck), and water with a mass ratio of 1:0.89:0.26 were mixed together. After the addition of the acid catalyst, the solution was continuously stirred at room temperature for 60 min and transformed to a sol. Subsequently, the base catalyst was added to the sol to increase the rate of silanol condensation leading to gel formation. Before gelation, the solution was transferred into a polymethylmethacrylate (plexiglass) rectangular mold (height = 7 cm, length = 5 cm, width = 1.3 cm) or a cylindrical plastic mold with varying dimensions (diameter = 2.45 cm, height = 5 cm or diameter = 1.2 cm, height = 10 cm) tightly sealed to prevent evaporation of the solvent. After the gelation, the resulting alcogels were soaked in an aging solution (40 v/v % TEOS, 10 v/v % water, 50 v/v % ethanol) at 50 °C in an oven for 24 h. The samples were further kept in TEOS aging solution at room temperature for varying times ranging from 1 day to 7 days to obtain aerogels with different densities. The alcogels were then washed in fresh ethanol for 3 days to remove any impurities and water remaining in the pores of the alcogels. Finally, the alcogels were dried at 40 °C and 100 bar with

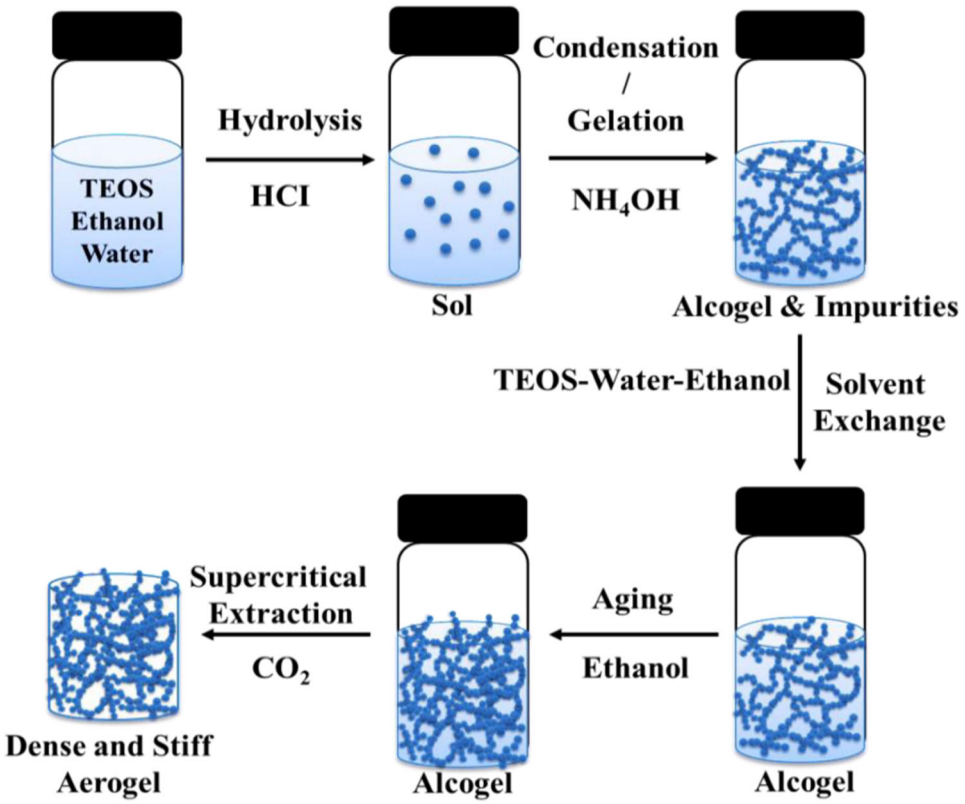

Fig. 2 Preparation of monolithic silica aerogels by aging silica alcogels in TEOS solution

supercritical CO_2 ($scCO_2$) in Applied Separations Speed SFE unit for 6 h.

2.2 Surface modification with hexamethyldisilazane (HMDS)

In order to render the aerogel surface hydrophobic, synthesized silica aerogel monoliths were treated with hexamethyldisilazane (HMDS) vapor in a tightly sealed beaker with a volume of 200 ml (Fig. 3). A stainless-steel screen was put in the middle of the beaker where liquid HMDS was placed to prevent contact between the aerogel and liquid HMDS. 6 mL of HMDS was placed at the bottom of the vessel while the aerogel was placed on top of the screen. The beaker was then sealed and heated to 110 °C at ambient pressure. The aerogels were exposed to HMDS vapor for around 3 h. After the treatment, unreacted HMDS and reaction products of HMDS with surface hydroxyl groups were removed by evaporation by keeping the samples in the oven at 120 °C for 1 h. At the end of the process, monolithic, crack-free hydrophobic silica aerogels were obtained.

2.3 Channel formation in aerogel monoliths

Cylindrical microchannels were created in hydrophobic aerogel monoliths by manual drilling using a drill bit (diameter = 2.1 mm, length = 4 cm). Figure 4a demonstrates how a straight channel was created within the aerogel block without cracking it and while preserving its monolithic structure. First, the sample was properly fixed. The hand-driven drill bit was then put perpendicularly to the aerogel surface and—while rotating continuously—moved slowly into the sample to prevent stress buildup. A straight channel with a diameter of ~2.1 mm was opened. An inclined *L*–shaped channel consisting of one horizontal channel intersecting with an inclined channel was also created as shown in Fig. 4b. First, a straight horizontal channel was drilled parallel to the sample axis in the *x* direction, creating a hole in the lateral face of the monolith. Subsequently, another channel was delicately drilled starting from the top face of the monolith and proceeding at an angle with respect to the normal direction of the top aerogel face up to the end of the initially created straight horizontal channel. The side view of the resulting inclined *L*-shaped channel is depicted in Fig. 4c.

2.4 Characterization of silica aerogels

Pore properties of the samples were determined by N_2 adsorption–desorption measurements at 77 K (Micromeritics ASAP 2020). The surface areas of the samples were determined by Brunauer−Emmett−Teller (BET) method whereas the pore volumes and pore size distributions were determined with Barrett−Joyner−Halenda (BJH)

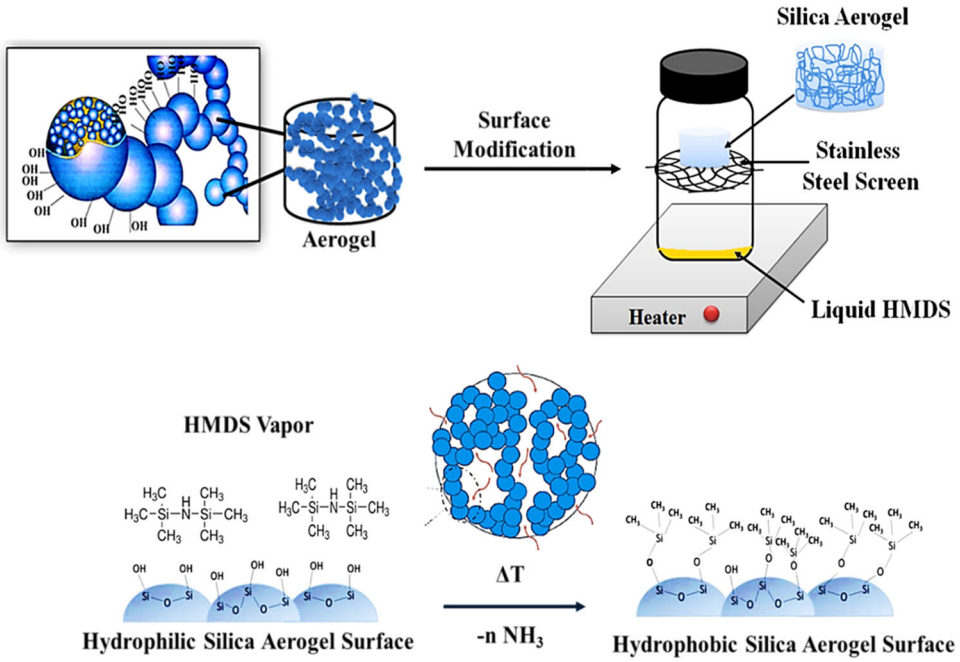

Fig. 3 Silanization of silica aerogel surface by vapor-phase deposition of HMDS

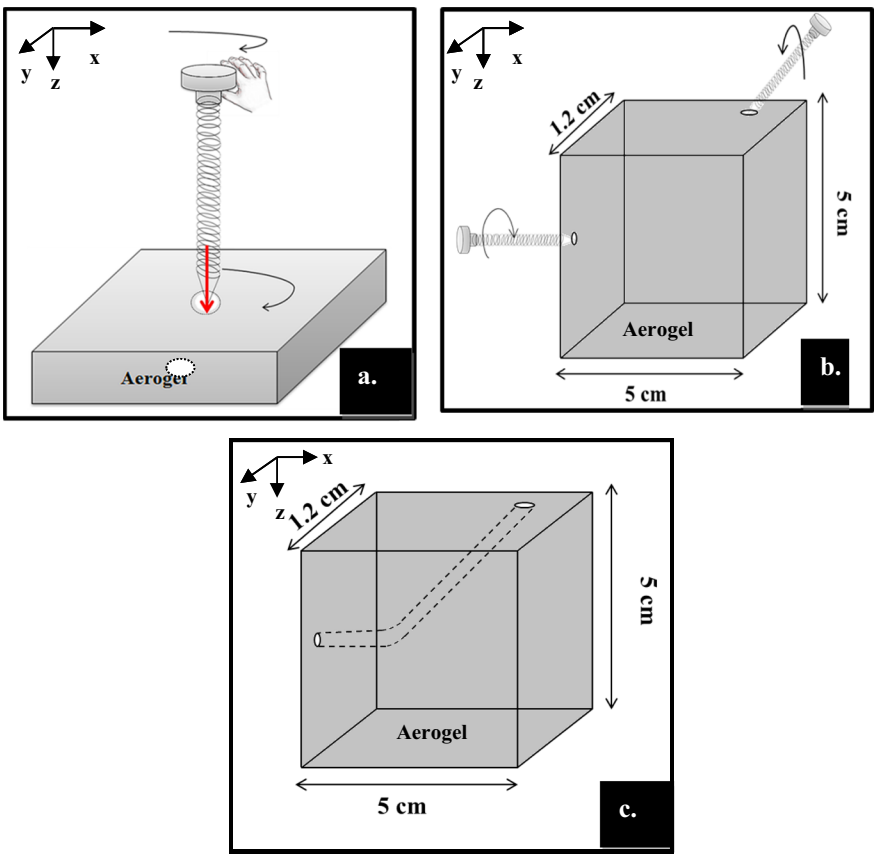

Fig. 4 **a** Straight-channel formation in aerogel by manual drilling **b** *L*-shaped channel formation in aerogel by manual drilling **c** Side-view of inclined *L*-shaped channel in monolithic aerogel

analysis from the N_2 adsorption−desorption isotherms with a relative pressure (P/P_0) ranging from 10^{-7} to 1 atm. Prior to analysis, samples were first degassed at 300 °C for 1 day to remove remaining impurities from the sample surfaces. Bulk density of each monolithic aerogel sample was determined by dividing its mass with its final volume which was determined by measuring the physical dimensions of the aerogel using a caliper. Hydrophobicity of the HMDS-

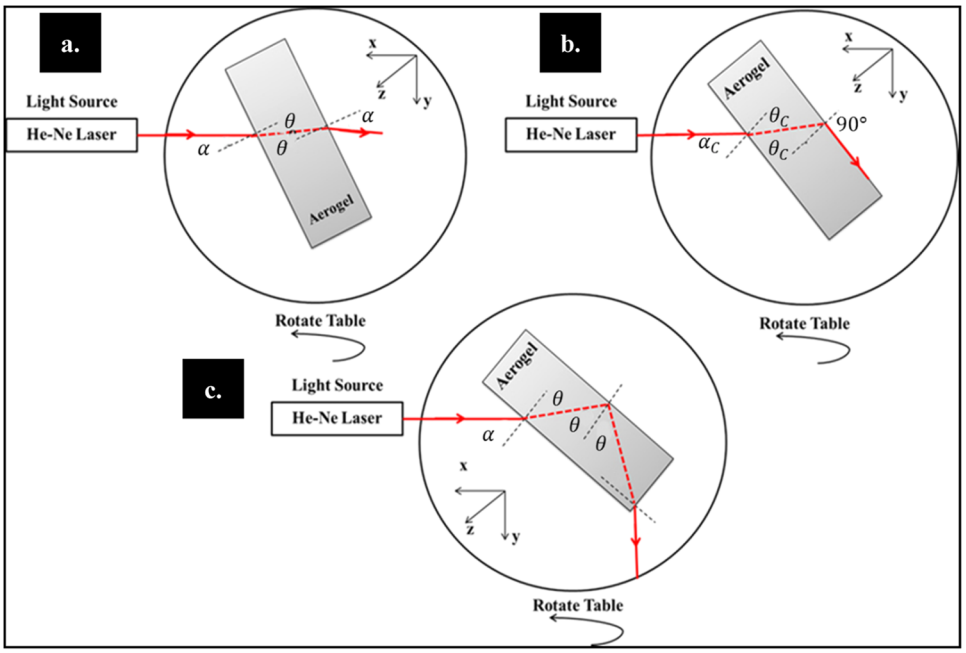

Fig. 5 Top view of experimental set-up for the measurement of silica aerogel refractive index

treated aerogels was quantified by contact angle measurements based on direct imaging of water droplets deposited on the surface of the samples. Static contact angle measurements were performed on a Krüss G-10 goniometer, fitted with a high resolution digital camera (Spot Insight Color; Diagnostic Instruments, Inc.) at room temperature (23 ± 1 °C). For contact angle measurements, 10 µL of deionized, triple distilled water was used. Wetting properties of the channel walls were also characterized by cutting the aerogel sample along the channel axis and dropping a water droplet directly on the channel surface. Refractive index of aerogel samples was measured by characterizing the refraction of a laser beam from aerogel monoliths placed on a goniometer stage. A laser beam from a He-Ne laser source (wavelength 632.8 nm) was coupled to the lateral face of the sample as shown in Fig. 5. The laser source was placed at a fixed position while the sample stage was slightly rotated in order to change the angle of incidence α of the laser beam on the front surface of the monolith. The light beam incident from air was refracted at the interface and propagated into the aerogel at an angle θ with respect to the surface normal. Since the front and rear surfaces of the aerogel monolith were parallel, angle of refraction θ was also equal to the angle of incidence on the rear surface of the aerogel. For θ smaller than the critical angle θ_c of the interface between the aerogel and air, the light was mostly refracted back into air at the rear surface of the aerogel block (Fig. 5a). As the sample was rotated counterclockwise, angle of incidence on the rear surface of the aerogel block increased and eventually became equal to the critical angle θ_c; at this condition, the refracted ray emerges at 90 ° with respect to the rear surface normal (Fig. 5b). When the sample was rotated a bit more, the ray incident on the rear surface of the monolith was totally internally reflected back into the aerogel, without emerging from the rear side of the aerogel into air (Fig. 5c). Refractive index of the aerogel was then calculated by using Eq. 1 and the measured critical angle θ_c, assuming $n_{\text{air}} = 1$:

$$n_{aerogel} = \frac{n_{air}}{\sin \theta_c} \tag{1}$$

A UV-VIS spectrophotometer (Shimadzu UV-3600) with a halogen lamp and deuterium lamp as irradiation sources was used to measure the absorbance of samples in the wavelength range of 350–1800 nm. Total luminous transmittance and diffuse transmittance were also measured using an integrating sphere attached to the UV-VIS spectrophotometer. For both measurements, the characterized aerogel was placed in front of the input port of the integrating sphere through which the light beam enters. When measuring the total transmittance, the sphere collected all the light passing through the aerogel sample. For diffuse transmittance measurements, the same arrangement as in the total luminous transmittance measurements was used, but the light passing without deflection straight through the aerogel was not collected due to the presence of an opening in the wall of the integrating sphere exactly opposite to the input port.

2.5 Characterization of optofluidic waveguides

A schematic diagram of the experimental setup used for the characterization of liquid-core optofluidic waveguides fabricated in monolithic aerogels is given in Fig. 6. A small

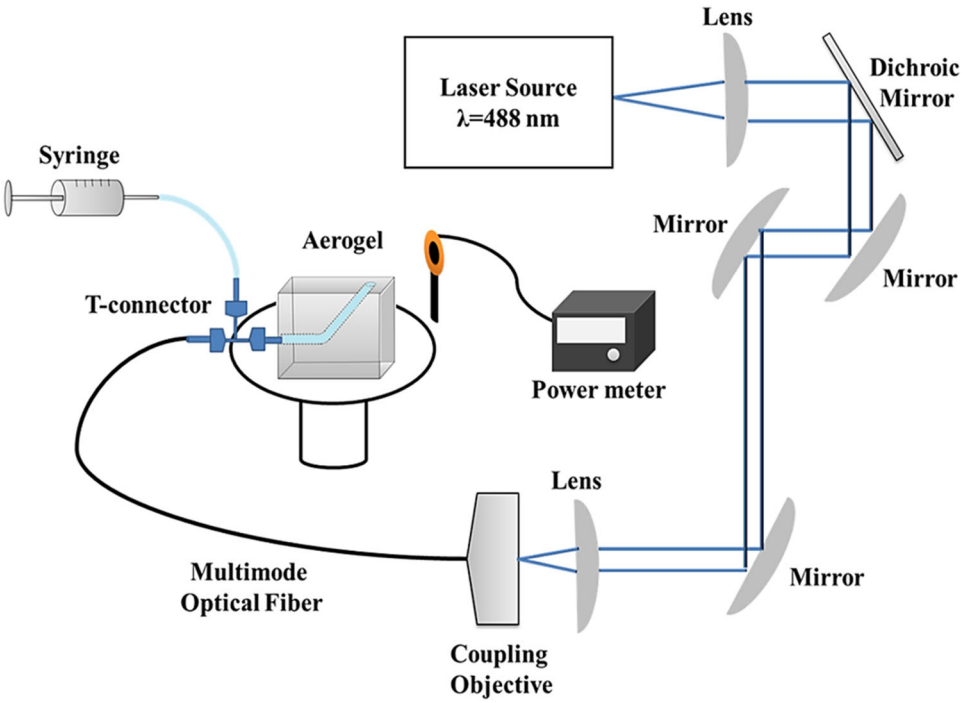

Fig. 6 Schematics of the experimental setup used in the characterization of light guiding in liquid-core optofluidic waveguides

piece of plastic tubing was glued to the input end of the channel drilled in the aerogel block by epoxy and the other end of the tubing was connected to a Union Tee adapter. Central port of the Union Tee was then connected to a syringe and the remaining end of the Union Tee was used to insert a solarization-resistant multimode optical fiber with a large core that served for coupling light into the channel. For the experiments, the aerogel was mounted in an adjustable metal holder. The channels formed in hydrophobic aerogels were filled with water by injection from the syringe. The microchannel was then illuminated by coupling a laser beam into the multimode optical fiber that subsequently delivered the light to the channel. The light at the operating wavelength of 488 nm from a frequency-doubled femtosecond-pulsed Ti:Sa solid-state laser source (Coherent Chameleon, maximum output power of 4 W at 800 nm) was coupled into the optical fiber with the aid of an objective lens. For the experiments, typical input power coupled into the optofluidic waveguide was 10 mW. The intensity of light transmitted through the waveguide was visually monitored and measured at the output end of the channel by a calibrated optical power meter.

3 Results and discussion

3.1 Properties of synthesized aerogel samples

The samples aged in TEOS-based solution for varying periods resulted in aerogels with different densities as shown in Table 1. The sample aged for 1 day had the lowest density of 0.15 g/cm^3, the sample aged for 2 days had a density of 0.22 g/cm^3 and the density of the sample aged for 7 days was 0.39 g/cm^3. As the aging time increased, further condensation reactions took place and additional silica monomers from the aging solution were introduced to the already formed silica network and increased solid content in the network. These additional condensation reactions enhanced the mechanical strength and stiffness of the resulting aerogel.

After performing the silanization of surface silanol groups with HMDS vapor, hydrophobicity of the samples was determined by measuring water contact angle on the silanized aerogel surfaces. As shown in Figs. 7a and b, average contact angles on the aerogel surface were 148.0° ± 3.6° (for aerogel density 0.15 g/cm^3) and 147.0° ± 1.8° (for aerogel density 0.22 g/cm^3), indicating that the samples were quite hydrophobic. Furthermore, their hydrophobic nature was preserved during the experiments over several weeks as water did not penetrate into the aerogel pores and did not crack the samples in the course of time.

Typical pore properties of the synthesized aerogels characterized by using nitrogen physisorption are tabulated in Table 2. As the sample density increased, BET surface area, BJH desorption average pore radius and total pore volume of the sample decreased. The pore volume, the surface area, and the average pore radius of the low-density sample (0.15 g/cm^3) were 3.6 cm^3/g, 662 m^2/g, and 11.1 nm, respectively. The sample with the highest density

Table 1 Properties of HMDS-treated aerogel samples of various density

Sample	Density (g/cm^3)	Porosity (%)	Measured refractive index	Critical angle (°)	Absorption coefficient (cm^{-1}) at 488 nm
1	0.15	93	1.023 ± 0.004	77.7 ± 1.1	0.52
2	0.22	90	1.060 ± 0.007	70.7 ± 1.0	0.69
3	0.39	82	1.093 ± 0.001	66.2 ± 0.1	0.87

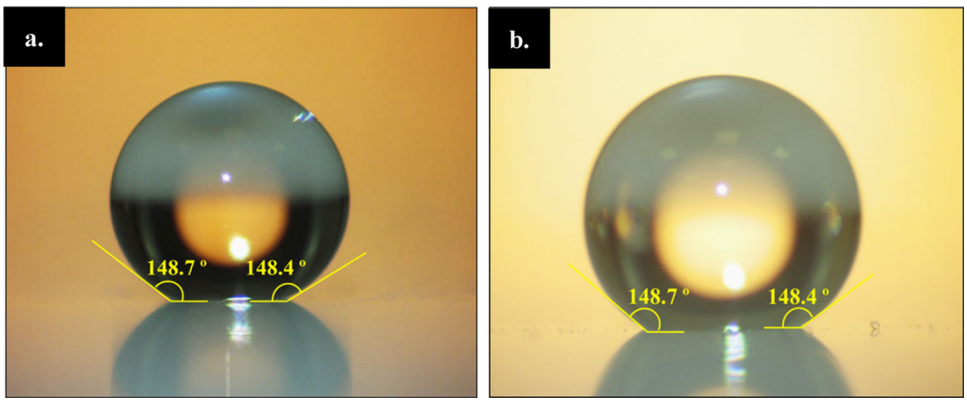

Fig. 7 **a** Water droplet resting on the surface of hydrophobic silica aerogel, $\rho = 0.15$ g/cm^3 **b** Water droplet resting on the surface of hydrophobic silica aerogel, $\rho = 0.22$ g/cm^3

(0.39 g/cm^3) had a significantly lower pore volume and pore radius of 0.35 cm^3/g and 1.4 nm, respectively.

The measured refractive indices of the samples at 632.8 nm are given in Table 1. In agreement with the expected behavior, they increased with increasing density of the aerogel, as the optical density characterized by the index of refraction is directly proportional to the material density. The refractive index of each sample was sufficiently lower than that of the core liquid water ($n_{H_2O} = 1.33$) making each one of them suitable for waveguide cladding.

As a measure of their light-gathering ability, NAs of the optical waveguides in aerogels were determined using Eq. 2 [23]:

$$NA = \sqrt{{n_{core}}^2 - {n_{cladding}}^2} \quad (2)$$

where n_{core} is the refractive index of the liquid in the microchannel and n_{cladding} is the refractive index of the cladding.

Water-filled multimode optofluidic waveguides in the synthesized aerogels yielded high numerical aperture values of 0.85, 0.81, and 0.76, ranking from the lowest to the highest aerogel density. In comparison, numerical aperture of doped silica fibers is typically around 0.37 and around 0.66 in Teflon-coated optical fibers [34]. Aerogel-based optofluidic waveguides with high numerical aperture collect light very efficiently when the light is coupled into the liquid core from a wide input angle and distribute light into a broad angle at the output.

Besides, absorption coefficients of the samples (a) were determined from the sample thickness (t) and absorbance (A) at the working wavelength (488 nm) using Eq. 3 [35]:

$$a = 2.303 \times A/t \quad (3)$$

Using the measured absorbance values at 488 nm from Fig. 8 and thicknesses of individual samples 1–3 ($t_1 = 1.2$ cm, $t_2 = 1.2$ cm, $t_3 = 1.7$ cm), the values of the absorption coefficients were calculated as $a_1 = 0.52$ cm^{-1}, $a_2 = 0.69$ cm^{-1} and $a_3 = 0.87$ cm^{-1}, respectively. These values are still relatively low compared to the common cladding materials such as polytetrafluoroethylene (PTFE) [36, 37]. For instance, transmission spectrum of a PTFE film with a thickness of 0.1 mm and a refractive index of 1.4 indicates that transmission of Teflon is lower than 10 % at 488 nm, which results in the absorbance around 1 and the absorption coefficient of the film about 230 cm^{-1} [37]. Thus, even the highest density aerogel samples have a lower absorption coefficient than PTFE. Furthermore, it was found that the diffuse transmittance and the total transmittance at 488 nm increased with decreasing density of the samples as shown in Fig. 9.

3.2 Channel formation in aerogel blocks

Images of channels created in hydrophobic aerogel blocks by manual drilling are shown in Figs. 10a–d. Relatively long channels (~7.5 cm) could be created with varying geometries such as straight and L-shaped inclined channels, while maintaining the nanoporous and monolithic structure of the aerogels blocks.

Table 2 Pore characteristics of HMDS-treated aerogel samples of various density

Sample	BET surface area (m^2/g)	BJH desorption average pore radius (nm)	Total pore volume (cm^3/g)
Silica aerogel ($\rho = 0.15$ g/cm^3)	662	11.1	3.61
Silica aerogel ($\rho = 0.22$ g/cm^3)	549	7.5	2.48
Silica aerogel ($\rho = 0.39$ g/cm^3)	467	1.4	0.35

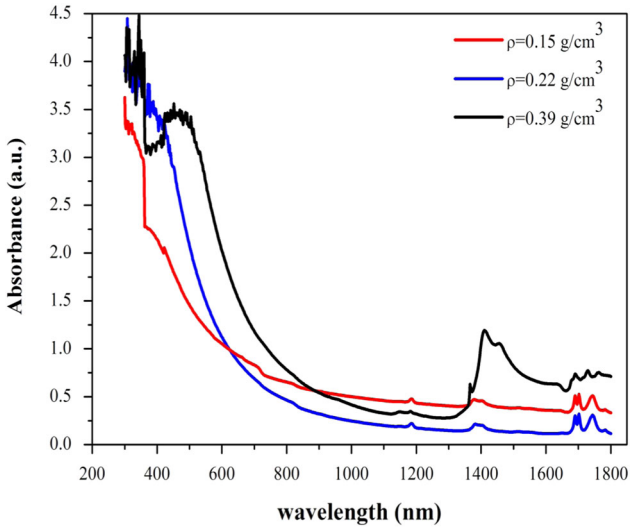

Fig. 8 Absorption spectra of synthesized aerogel samples of various densities

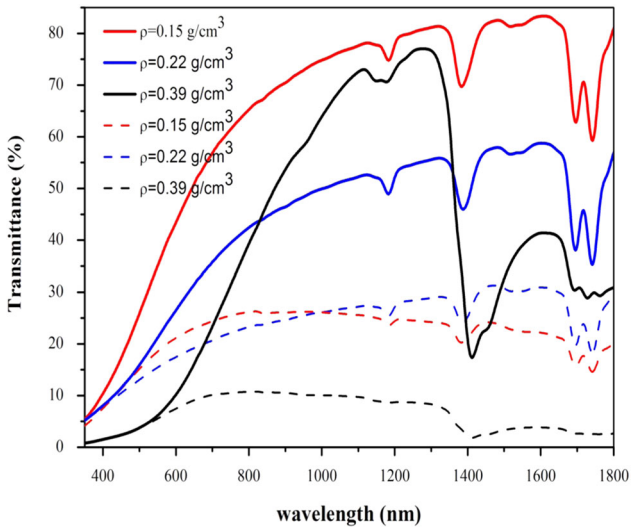

Fig 9 Total transmittance spectrum (*solid lines*) and diffuse transmittance spectrum (*dashed lines*) of synthesized aerogel samples of various densities in the spectral range between 350–1800 nm

3.3 Light-guiding in liquid-core optofluidic waveguides in aerogels

Following the successful microchannel formation inside the aerogel blocks, multimode optofluidic waveguides were generated by filling the channels with water as the core liquid. The channel was filled with water by using a syringe as described in Section 2.6. Water could be confined within the channels with hydrophobic walls without penetrating the porous network of the aerogel.

Laser light with the wavelength of 488 nm was coupled into the optical waveguide in the aerogel ($\rho = 0.15$ g/cm^3) with the aid of the optical fiber, as shown schematically in Fig. 6 in Section 2.6. As the light propagates inside the channel, some of the propagating light rays which strike the boundary between water and the aerogel at an angle greater than the critical angle are reflected back to the opposite wall of the channel (Figs. 11 and 12b). As illustrated in the photograph of the channel with coupled light shown in Fig. 11, the light was totally internally reflected in the channel several times after emerging from the input fiber, before leaving the waveguide. Consecutive reflections appear more faintly as the light intensity decreases during the propagation through light scattering and absorbance by the aerogel.

The expected number and spacing of subsequent reflections of a ray from the channel walls during the light propagation was also estimated using Snell's Law with the output half-angle α of the optical fiber immersed in water calculated from the numerical aperture of the fiber. Figure 12a illustrates light transmission through an optical fiber inserted into water. Because the numerical aperture of the fiber is preserved regardless of the medium outside the fiber, angle α can be determined from $NA = n_{water} \sin \alpha$ where NA is the numerical aperture of the fiber (NA = 0.22) [38] and $n_{water} = 1.33$. Inserting these values then gives $\alpha = 9.5°$. From Fig. 12b, the angle β at which the light is reflected from the microchannel wall back into water can be calculated as $\beta = 90° - \alpha = 80.5°$. From the geometry of the configuration (channel diameter $D = 2.1$ mm, fiber core diameter $d = 0.3$ mm), the light exiting the fiber propagates over a lateral distance $\Delta = (D-d)/2 = 0.9$ mm before the first incidence on the channel wall. This corresponds to the distance x between the fiber tip and the point where the wave first strikes the channel wall equal to $x = \Delta \tan \beta = 5.4$ mm. The distance in the axial direction over which the light propagates between successive reflections is then $2x = 10.8$ mm. For a channel with the length of 27 mm, it was found

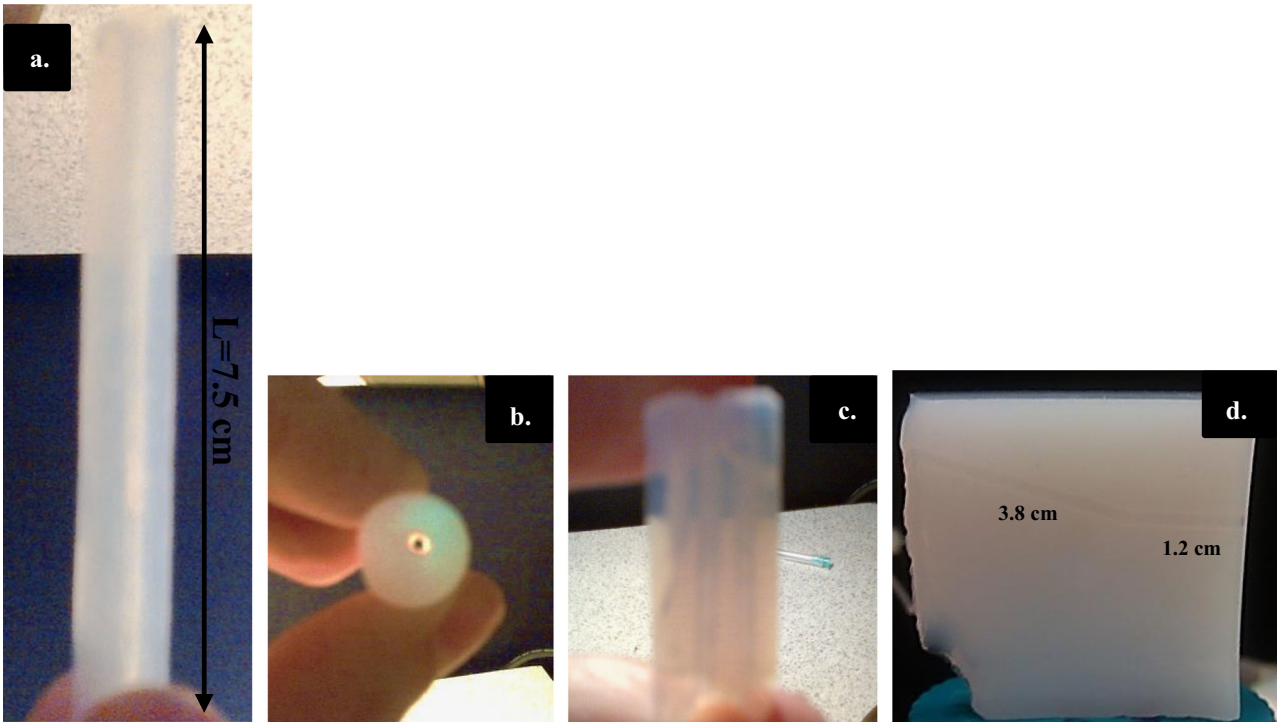

Fig. 10 **a**. Side view of a hydrophobic silica aerogel rod with a channel parallel to the rod axis (channel length $L = 7.5$ cm, channel diameter $D = 2.1$ mm) **b**. Top-view of the aerogel rod shown in **a** with a channel parallel to the rod axis **c**. Silica aerogel sample with multiple channels **d**. Side view of a L-shaped channel with one horizontal and one inclined channel (channel lengths $L_1 = 1.2$ cm and $L_2 = 3.8$ cm, respectively; channel diameters $D_1 = D_2 = 2.1$ mm)

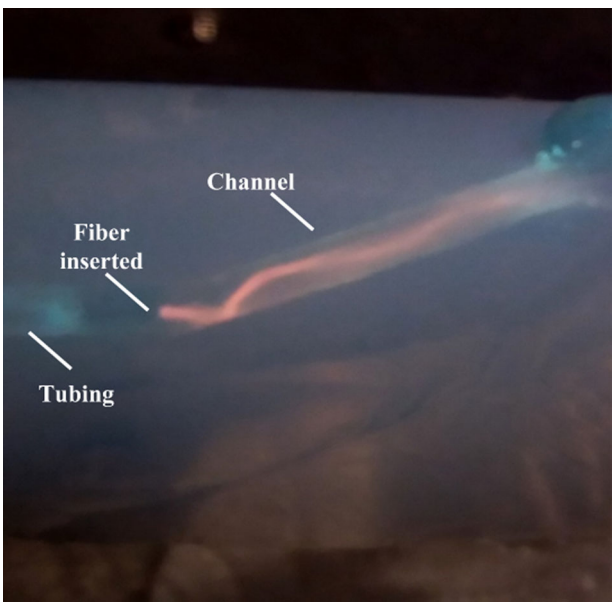

Fig. 11 Total internal reflection in the water-filled channel in a monolithic aerogel ($\rho = 0.15$ g/cm^3)

that a ray of light can do about three total internal reflections at most, neglecting intensity loss. As demonstrated in Fig. 11, this is in agreement with experimental observation.

The same phenomena could also be observed with inclined *L*-shaped waveguides fabricated in denser aerogel samples (see Fig. 10d). In the experiments, the laser light was coupled into the horizontal part of the channel and the transmitted light was collected from the open end of the inclined part of the channel. When the light was coupled into an empty channel, no guiding of light to the opposite end of the channel was observed; instead, the light was scattered strongly from the junction of the two sections of the channel (see Fig. 13a). Upon filling the channel with water, situation changed dramatically and the waveguides became fully operational. As shown in Fig. 13b, for water-filled channel, the light was guided along the channel and delivered to the opposite end of the channel (seen at the top of the aerogel block). A side-view image of water filled channel with light coupling in Fig. 13b. demonstrates that the entire length of the channel is filled with light with a bright spot on the top which indicates that the light is transmitted along the liquid-core optofluidic waveguide. Because of the opacity of dense aerogels, straight path of the light through the aerogel is not well visible; however, scattering of light beam at the edges of the channel can be clearly observed.

Overall losses of water-filled *L*-shaped waveguides were quantified by measuring the power of the transmitted light using a power meter. At the wavelength of 488 nm, output

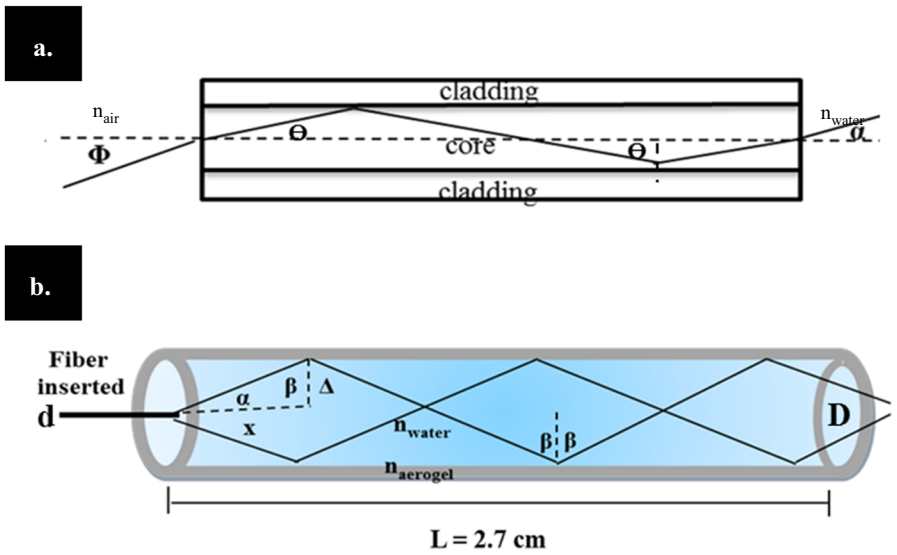

Fig. 12 **a** Light propagation through an optical fiber inserted into a water-filled channel in aerogel. A ray with the maximum acceptance half-angle of the fiber in air (Φ) is coupled into the fiber and subsequently propagates along the fiber and emerges with angle (α) into water. **b**. Total internal reflection in the microchannel. *d* is the diameter of the fiber core (0.3 mm), *D* is the diameter of the microchannel (2.1 mm)

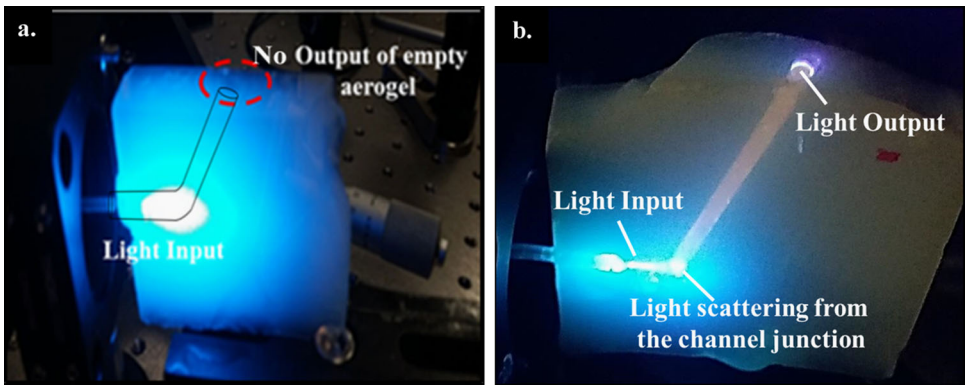

Fig. 13 **a**. Light coupling into an empty channel in the aerogel **b**. Light propagation in liquid-filled channel within the aerogel monolith (side view)

power of 2.1 mW was measured when the laser light was coupled with an incident power of 8.0 mW from the fiber output. The overall optical throughput of the optical waveguide can be quantified by Eq. 4 in terms of the input optical power, P_0, and the output power, $P(z)$, observed after the light propagates a distance, z, along the waveguide length:

$$P(z)=P_0 e^{-\propto_{total} z} \tag{4}$$

where α_{total} is the total attenuation coefficient (involving all contributions to attenuation).

α_{total} was obtained as 0.33 cm^{-1}, assuming a waveguide length of ~4 cm. Hence, the propagation loss of the waveguide, η, can be calculated as −1.45 dB/cm by Eq. 5:

$$\eta = -\frac{10\propto_{total}}{ln10} \tag{5}$$

This value compares favorably to the previously measured propagation loss of −9.9 dB/cm for liquid-core optofluidic waveguide prepared using laser ablation in silica aerogels [23].

The loss in power is primarily due to the light scattering at the junction of the two channel sections since the vertical part of the channel is inclined with an angle of 62° and most of the rays possibly strike the channel surface with the incident angle smaller than the critical angle (71. 4°). They are therefore partially reflected or transmitted in many different directions, leaving a bright spot clearly visible at the channel junction (see Fig. 13b). If the inclined channel is formed with a moderate angle around 20°, light-guiding efficiency can possibly be improved. Furthermore, light intensity also decreases during subsequent reflections at the channel walls due to the surface roughness. Absorption loss by water at 488 nm is low and it transmits within water with 0.05% incident light attenuation for 1 cm length [39]. Thus, the use of water as the core liquid does not represent the main limitation on the performance of our optofluidic waveguides.

4 Conclusions

Multimode liquid-core optofluidic waveguides based on total internal reflection of light in water-filled microchannels

located within high-density hydrophobic silica aerogels were fabricated by direct mechanical drilling. The synthesized aerogel samples with high densities had still sufficiently low refractive indices and absorption coefficient values, exhibiting ideal optical cladding material properties for efficient guiding of light by total internal reflection over a wide range of wavelengths without the use of any additional optical coatings. Relatively long channels of various shapes (straight and inclined *L*-shape) were created preserving the nanoporous and monolithic structure of the aerogel. Water-filled multimode optofluidic waveguides in the synthesized aerogels provided high numerical aperture values making them ideal for applications involving aqueous liquid cores. Efficient wave-guiding upon light coupling (at 488 nm) into the water-filled channel and channel output could be demonstrated. The total internal reflection phenomena within the water-filled channel in the hydrophobic aerogel as a multimode core waveguide could also be visually revealed. Therefore, the demonstrated fabrication technique could enable the use of aerogel-based optofluidic waveguides for innovative applications including photochemical reactions as well as light-driven detection, identification, and quantification of particular chemical compounds and metabolic variables with the aid of improved light distribution through the reaction space represented by the waveguide core.

Acknowledgements We thank KUYTAM (Koç University Surface Science and Technology Center) and KUTEM (Koç University TÜPRAŞ Energy Center) for their support.

Compliance with ethical standards

Conflict of interest The authors declare that they have no competing interests.

References

1. Monat C, Domachuk P, Eggleton BJ (2007) Integrated optofluidics: a new river of light. Nat Photon 1(2):106–114
2. Psaltis D, Quake SR, Yang C (2006) Developing optofluidic technology through the fusion of microfluidics and optics. Nature 442(7101):381–386
3. Pang L, Chen HM, Freeman LM, Fainman Y (2012) Optofluidic devices and applications in photonics, sensing and imaging. Lab Chip 12(19):3543–3551
4. Lei L, Wang N, Zhang XM, Tai Q, Tsai DP, Chan HL (2010) Optofluidic planar reactors for photocatalytic water treatment using solar energy. Biomicrofluidics 4(4):43004
5. Erickson D, Sinton D, Psaltis D (2011) Optofluidics for energy applications. Nat Photon 5(10):583–590
6. Korampally V, Mukherjee S, Hossain M, Manor R, Yun M, Gangopadhyay K, Polo-Parada L, Gangopadhyay S (2009) Development of a miniaturized liquid core waveguide system with nanoporous dielectric cladding—A potential biosensing platform. IEEE Sens J 9(12):1711–1718
7. Manor R, Datta A, Ahmad I, Holtz M, Gangopadhyay S, Dallas T (2003) Microfabrication and characterization of liquid core waveguide glass channels coated with Teflon AF. IEEE Sens J 3 (6):687–692
8. Parks JW, Schmidt H (2016) Flexible optofluidic waveguide platform with multi-dimensional reconfigurability. Sci Rep 6:33008
9. Cristiano MBC, Christiano JSdM, Eliane MdS, Alexandre B, Jackson SKO, Tilon F, Giancarlo C, Alfredo RV, Carlos HBC (2007) Towards practical liquid and gas sensing with photonic crystal fibres: side access to the fibre microstructure and single-mode liquid-core fibre. Meas Sci Technol 18(10):3075
10. Fan X, White IM (2011) Optofluidic microsystems for chemical and biological analysis. Nat photonic 5(10):591–597
11. Ozcelik D, Parks JW, Wall TA, Stott MA, Cai H, Parks JW, Hawkins AR, Schmidt H (2015) Optofluidic wavelength division multiplexing for single-virus detection. Proc Natl Acad Sci U S A 112(42):12933–12937
12. Ellis PS, Gentle BS, Grace MR, McKelvie ID (2009) A versatile total internal reflection photometric detection cell for flow analysis. Talanta 79(3):830–835
13. Shih-Hao H, Fan-Gang T (2005) Development of a monolithic total internal reflection-based biochip utilizing a microprism array for fluorescence sensing. J Micromech Microeng 15(12):2235
14. Jung JH, Lee KS, Im S, Destgeer G, Ha BH, Park J, Sung HJ (2016) Photosynthesis of cyanobacteria in a miniaturized optofluidic waveguide platform. RSC Adv 6(14):11081–11087
15. Ramachandran S, Cohen DA, Quist AP, Lal R (2013) High performance, LED powered, waveguide based total internal reflection microscopy. Sci Rep 3:2133
16. Dallas T, Dasgupta PK (2004) Light at the end of the tunnel: recent analytical applications of liquid-core waveguides. Trends Anal Chem 23(5):385–392
17. Schelle B, Dreß P, Franke H, Klein KF, Slupek J (1999) Physical characterization of lightguide capillary cells. J Phys D Appl Phys 32(24):3157
18. Bernini R, Campopiano S, Zeni L, Sarro PM (2004) ARROW optical waveguides based sensors. Sens Actuators B Chem 100 (1–2):143–146
19. Hawkins AR, Schmidt H (2007) Optofluidic waveguides: II. Fabrication and structures. Microfluid Nanofluidics 4(1–2):17–32
20. Özbakır Y, Jonas A, Kiraz A, Erkey C (2017) Aerogels for optofluidic waveguides. Micromachines 8(4):98
21. Schmidt H, Hawkins AR (2008) Optofluidic waveguides: I. Concepts and implementations. Microfluid Nanofluidics 4 (1):3–16
22. Hawkins AR, Schmidt H (2008) Optofluidic waveguides: II. Fabrication and structures. Microfluid Nanofluidics 4(1):17–32
23. Yalizay B, Morova Y, Dincer K, Ozbakir Y, Jonas A, Erkey C, Kiraz A, Akturk S (2015) Versatile liquid-core optofluidic waveguides fabricated in hydrophobic silica aerogels by femtosecond-laser ablation. Opt Mater 47:478–483
24. Datta A, In-Yong E, Dhar A, Kuban P, Manor R, Ahmad I, Gangopadhyay S, Dallas T, Holtz M, Temkin H, Dasgupta PK (2003) Microfabrication and characterization of teflon AF-coated liquid core waveguide channels in silicon. IEEE Sens J 3 (6):788–795
25. Wu CW, Gong GC (2008) Fabrication of PDMS-based nitrite sensors using Teflon AF coating microchannels. IEEE Sens J 8 (5):465–469. doi:10.1109/JSEN.2008.918201
26. Cho SH, Godin J, Lo YH (2009) Optofluidic waveguides in Teflon AF-coated PDMS microfluidic channels. IEEE Photon Technol Lett 21(15):1057–1059
27. Datta A, Eom IY, Dhar A, Kuban P, Manor R, Ahmad I, Gangopadhyay S, Dallas T, Holtz M, Temkin F, Dasgupta PK (2003) Microfabrication and characterization of Teflon AF-coated

liquid core waveguide channels in silicon. IEEE Sens J 3 (6):788–795
28. Hüsing N, Schubert U (1998) Aerogels—Airy Materials: chemistry, structure, and properties. Angew Chem Int Ed 37 (1–2):22–45
29. Du A, Zhou B, Zhang ZH, Shen J (2013) A special material or a new state of matter: a review and reconsideration of the aerogel. Materials 6(3):941–968. doi:10.3390/ma6030941
30. Bellunato T, Calvi M, Matteuzzi C, Musy M, Perego DL, Storaci B (2007) Refractive index dispersion law of silica aerogel. Eur Phys J C 52(3):759–764
31. Xiao L, Birks TA (2011) Optofluidic microchannels in aerogel. Opt Lett 36(16):3275–3277
32. Eris G, Sanli D, Ulker Z, Bozbag SE, Jonás A, Kiraz A, Erkey C (2013) Three-dimensional optofluidic waveguides in hydrophobic silica aerogels via supercritical fluid processing. J Supercrit Fluids 73:28–33
33. Bian Q, Chen S, Kim B-T, Leventis N, Lu H, Chang Z, Lei S (2011) Micromachining of polyurea aerogel using femtosecond laser pulses. J Non-Cryst Solids 357(1):186–193
34. Issa NA (2004) High numerical aperture in multimode microstructured optical fibers. Appl Opt 43(33):6191–6197
35. Djouadi D, Meddouri M, Chelouche A (2014) Structural and optical characterizations of ZnO aerogel nanopowder synthesized from zinc acetate ethanolic solution. Opt Mater 37:567–571
36. Thorlabs (1999) Optical Substrates. Accessed 16 November 2017
37. Riedel D, Castex MC (1999) Effective absorption coefficient measurements in PMMA and PTFE by clean ablation process with a coherent VUV source at 125 nm. Appl Phys A 69(4):375–380
38. Thorlabs (1999) Multimode Fiber Optic Patch Cables. Accessed 16 November 2017
39. Pope RM, Fry ES (1997) Absorption spectrum (380–700 nm) of pure water. II. Integrating cavity measurements. Appl Opt 36 (33):8710–8723